Author/s:
Blunck, Y;Moffat, BA;Kolbe, SC;Ordidge, RJ;Cleary, JO;Johnston, LA

Title:
Zero-gradient-excitation ramped hybrid encoding (zGRF-RHE) sodium MRI

Date:
2019-02-01

Citation:
Blunck, Y., Moffat, B. A., Kolbe, S. C., Ordidge, R. J., Cleary, J. O. & Johnston, L. A. (2019). Zero-gradient-excitation ramped hybrid encoding (zGRF-RHE) sodium MRI. Magnetic Resonance in Medicine, 81 (2), pp.1172-1180. https://doi.org/10.1002/mrm.27484.

Persistent Link:
https://hdl.handle.net/11343/284517

MS. YASMIN BLUNCK (Orcid ID : 0000-0003-3600-9958)

Article type : Note

Zero-Gradient-Excitation Ramped Hybrid Encoding (zG_{RF}-RHE) Sodium MRI

Running title:

zG_{RF}-RHE Sodium MRI

Yasmin Blunck[1,2]*, Bradford A. Moffat[2], Scott C. Kolbe[2], Roger J. Ordidge[2], Jon O. Cleary[2†], Leigh A. Johnston[1,2†]

[1] *Biomedical Engineering, University of Melbourne, Parkville, Australia*

[2] *Melbourne Brain Centre Imaging Unit, Anatomy and Neuroscience, University of Melbourne, Parkville, Australia*

[†] *joint senior authors*

*correspondence: Melbourne Brain Centre Imaging Unit, Kenneth Myer Building, University of Melbourne, 30 Royal Parade, Parkville VIC 3052, Australia

email: blunck.yasmin@gmail.com

This is the author manuscript accepted for publication and has undergone full peer review but has not been through the copyediting, typesetting, pagination and proofreading process, which may lead to differences between this version and the Version of Record. Please cite this article as doi: 10.1002/mrm.27484

Key words: Sodium (^{23}Na) MRI; hybrid encoding; zero echo time (zTE); UTE; PETRA; RHE
Word count: 3455

Abstract

Purpose: Fast biexponential transverse signal decay compounds sodium image quality. This work aims at enhancing image characteristics using a special case of ramped hybrid encoding (RHE). Zero-gradient-excitation (zG_{RF})-RHE provides 1) gradient-free excitation for high flip angle, artifact-free excitation profiles and 2) gradient ramping during dead-time for the optimization of encoding time (t_{enc}) to reduce T_2^* signal decay influence during acquisition.

Methods: Radial zG_{RF}-RHE and standard radial UTE were investigated over a range of receiver bandwidths in simulations, phantom and in in vivo brain experiments. Central k-space in zG_{RF}-RHE was acquired through single point measurements at the minimum achievable TE. T_2^* blurring artifacts and image SNR and CNR were assessed.

Results: zG_{RF} -RHE enabled 90° flip angle artifact-free excitation, while gradient pre-ramping provided greater t_{enc} efficiency for any readout bandwidths. Experiments confirmed simulation results, revealing sharper edge characteristics particularly at short readout durations (T_{RO}). Significant SNR improvements of up to 4.8% were observed for longer T_{RO}.

Conclusion: zG_{RF} -RHE allows for artifact-free high flip angle excitation with time-efficient encoding improving on image characteristics. This hybrid encoding concept with gradient pre-ramping is trajectory independent and can be introduced in any center-out UTE trajectory design.

Introduction

Sodium (^{23}Na) plays a vital role in various processes and body functions. Cells keep up a delicate balance between intra- and extracellular sodium concentration – a mechanism that is strongly dependent on the cell's metabolism and its membrane integrity. Disturbances of

this delicate balance provide a sensitive, early indicator for cell breakdowns and give an insight into cell integrity and tissue viability. With sodium nuclei providing the second strongest MR-signal in biological tissue, sodium MRI offers promising potential as a clinical biomarker with capabilities ranging from early diagnosis to therapy response monitoring as well as the detection of diseases without anatomical abnormalities (1). Due to hardware advancements, the number of sodium MRI studies is steadily increasing (2) ranging across a variety of diseases encompassing stroke (3,4), tumors (5-7), neurodegenerative diseases (8,9), and musculoskeletal pathologies (10-12).

Nonetheless, sodium MRI suffers from comparatively low image quality related to two major challenges: a relatively low NMR sensitivity and a fast biexponential transverse signal decay. The latter requires sodium MRI data to be acquired with dedicated imaging techniques that allow for the measurement of ultra-short TE-values. This class of sequences is termed UTE imaging and is usually characterized by a short non-selective hard-pulse followed by data acquisition from the center of k-space towards its periphery. Due to the usually non-selective hard-pulse, sodium acquisitions are most commonly performed in 3D. There mainly exist two approaches for a quick center-out traversal through k-space: radial or twisted half-projections (13-15) and variations thereof (16,17).

Signal decay commences from the center of the excitation pulse, which consequently requires sampling to start as quickly as possible. However, the limited switching time between transmit and receive channel (dead-time) induces an inherent delay to the ADC onset; commonly ranging from 40 to 100 μs on clinical systems. UTE sequences furthermore synchronize the beginning of data sampling with gradient ramp-up. Due to finite gradient slew rates this acquisition strategy leads to a lower initial traversing speed and reduced sample spacing in k-space center resulting in generally increased encoding time (t_{enc}) for all k-space locations.

An improvement in t_{enc} can be achieved through zero echo time (zTE) imaging where gradients are ramped up prior to RF excitation (18). Such sequence design enables sampling under full gradient strength directly after ADC onset. However, since k-space

encoding is prescribed by gradient activation, zTE imaging schemes cannot readily collect central k-space data as it is immeasurable during the receiver dead-time. A special case of zTE acquisition are single point imaging (SPI) or constant imaging techniques like RASP (19) and SPRITE (20) where k-space is filled up pointwise on a Cartesian grid. Since each measurement can be acquired at a fixed t_{enc} the acquired signal is free from convolutional impact of T_2^*. However, the pointwise signal acquisition leads to clinically infeasible scan times. Pointwise Encoding Time Reduction with Radial Acquisition (PETRA) is a hybrid zTE technique which combines radial zTE with SPI in outer and inner k-space, respectively, and has shown to improve image SNR and reduce T_2^* blurring in imaging of short T_2 species (21).

While PETRA and other zTE imaging techniques have shown promising results, they are not commonly applied in sodium MRI. RF excitation in the presence of gradients requires a broad transmit bandwidth necessitating short excitation pulses. With limited B1 power, this leads to a reduced attainable flip angle. Violation of the bandwidth constraint results in variable and nonuniform excitation profiles. Nevertheless, Romanzetti et al. (22) demonstrated the application of SPRITE in sodium MRI and found that the signal loss due to the flip angle constraint can be partly overcome through averaging. However, overall SNR was lower than in standard UTE acquisitions.

Recent work by Jang et al. (23) suggests ramped hybrid encoding (RHE) – an extension to PETRA – by introducing a two-step gradient ramping: 1) initially gradients are ramped to an intermediate strength (G_{RF}) during which the RF pulse is applied; 2) immediately after excitation, gradients are ramped to their final strength for shortest k-space encoding. The flexible excitation and readout gradient setup mitigates slice selectivity effects and enables higher flip angles while still allowing for low t_{enc}.

In this work we investigate zG_{RF}-RHE – a special case of RHE – with zero G_{RF} and an immediate ramp-up after RF excitation, i.e. during dead-time. The missing k-space center is filled with single point measurements as in PETRA and RHE. Such imaging approach achieves optimized t_{enc} for any receiver bandwidth while still allowing high flip angle

excitation without any slice selectivity in the excitation profile. We show that the optimized encoding scheme leads to an increase in image SNR. For short readout duration a reduction in T_2^* blurring was observed.

Methods

Imaging Sequence

Sodium images were acquired with a custom-built 3D radial sequence based on Saff and Kuijlaar's method (24) for a homogeneous projection placement. The standard 3D radial UTE sequence consisted of a non-selective hard pulse followed by simultaneous gradient onset and data sampling after dead-time delay. The 3D radial zG_{RF}-RHE sequence (Figure 1) was composed of a non-selective hard pulse immediately followed by gradient ramping; data sampling commenced after dead-time. The dead-time was set to 100 μs, a common coil configuration for most clinical systems. The required gradient strength for image resolution and readout duration (T_{RO}) allowed for a full gradient ramp-up within dead-time. The data sampling dwell time was kept at 5 μs for both imaging sequences. Standard 3D radial UTE and zG_{RF}-RHE were compared with a constant receiver bandwidth. Throughout this paper, T_{RO} is stated with respect to the UTE sequence design. Due to the pre-ramping of gradients, the effective T_{RO} in zG_{RF}-RHE is reduced by the dead-time, i.e. $T_{RO,RHE} = T_{RO,UTE} - t_d$.

In zG_{RF}-RHE, the gap in central k-space was filled with single point acquisitions. It should be noted that all single point measurements were acquired under the same conditions as the projection measurements, i.e. with zero gradients during excitation and ramping during dead-time. Unlike PETRA, single points were therefore not measured with stepwise gradient increase, but with gradient ramp up and down between single point measurements. A diagram for zG_{RF}-RHE can be found in Figure 1.

Image Reconstruction

Images were reconstructed offline via Kaiser-Bessel re-gridding in MATLAB. The re-gridding oversampling factor was set to 1.5. Radial and single point measurements were combined for zG_{RF}-RHE reconstruction. An iterative density compensation was applied to the raw data from UTE and zG_{RF}-RHE measurements prior to re-gridding (25). Radial

projection rawdata were furthermore weighted with a Hann filter to reduce Gibbs ringing artifacts.

Simulations

The influence of encoding time and biexponential decay on image reconstruction was analyzed in a 1D simulation implemented in MATLAB. The profile was composed of tubes with varying sodium concentrations (0.4, 0.2, 0.3, 0.6 and 1.0) and tube diameters (6.2 mm, 12.4 mm and 24.8 mm). Simulation parameter were set to match the experimental sodium MR measurements: TE = 0.3 ms, dead-time = 0.1 ms, FOV = 20 cm and 3.1 mm image resolution. Reconstruction characteristics were investigated for T_{RO} of 2 and 8 ms. The profile was simulated for biexponential brain tissue signal decay properties with a fast component of 1.5 ms , a slow component of 20 ms and respective signal fractions of 0.6 and 0.4 (26).

MR Measurements

Imaging was performed on a research 7T MRI scanner (Siemens Healthcare, Erlangen, Germany) with a transmit/receive dual-tuned ^{1}H-^{23}Na head coil (QED, Mayfield Village, Ohio USA).

Phantom

SNR analysis and T_2^* blurring effects were investigated in phantom experiments. The phantom consisted of Falcon tubes with varying diameter (28, 14 and 6 mm) and saline concentrations (30 and 45 mM). All tubes were submerged in distilled water and filled with 3 % agarose gel to induce biexponential signal decay characteristics. Sodium images were acquired over an isotropic field of view of 20 cm with a nominal isotropic 3.1 mm resolution. Measurements were taken under 90° flip angle and a repetition time (TR) of 160 ms to reduce T1-weighting; 8000 radial projections lead to a total scan time 21 min 20 sec in UTE acquisitions, zG_{RF}-RHE measurements required additional scan time for single point measurements (at the chosen FOV and TR, up to 4.3 sec for T_{RO} = 2ms acquisition). The RF pulse length was 420 μs. Echo time (TE) was defined as the time interval between the center of the pulse and the onset of data sampling and was set to 0.31 ms. Images were

acquired at different T_{RO} (2, 4, 6 and 8 ms.) and measurements were repeated eight times for a statistical analysis of SNR effects.

Furthermore, a proton-based FLASH image was acquired with TR = 11 ms, TE = 3.06 ms, 14° flip angle, 1 mm isotropic resolution, acquisition time 6min 12sec.

B_0-field shimming was based on a vendor-provided 3D shimming routine and was performed on the proton channel. Shim optimization was repeated 5-10 times until shim settings converged.

In vivo

All human imaging was conducted with the approval of the University of Melbourne Human Research Ethics Committee and volunteers gave an informed consent prior to the experiment. Human in vivo acquisitions were performed on one healthy female volunteer. Sodium and proton imaging parameters as well as the shimming procedure were identical to the phantom experiments. The volunteer was imaged with 3D radial UTE and 3D radial zG_{RF}-RHE with T_{RO} of 2 ms providing good SNR at a high bandwidth for the chosen image resolution (27).

SNR analysis

Given the low signal regime of sodium images, SNR measurements from magnitude images were calculated based on Gudbjartsson and Patz' Rician noise correction scheme (28). Magnitude image intensities were corrected according to

$$A = \sqrt{|M^2 - \sigma^2|}$$

where A and M are the corrected and magnitude image intensities, respectively, and σ the noise standard deviation in the real or imaginary image. SNR measurements were taken from a central ROI within the large (28 mm diameter) phantom vials. The smaller phantom vials were excluded from the statistical SNR analysis due to strong partial volume effects. The analysis of a central region within a larger object is expected to provide higher measurement accuracy (29). A Student's t-test was applied to the ROIs across all eight measurements for a statistical analysis of SNR effects.

Results

The simulation results are shown in Figure 2. The Modulation Transfer Function (MTF) is the frequency space counterpart of the point spread function and describes the contrast of spatial frequencies under t_{enc} and signal decay. Figure 2 (a) illustrates the MTF and t_{enc} for 2 and 8 ms T_{RO} under biexponential signal decay as it occurs in brain tissue (T_{2s}= 1.5 ms, T_{2l} = 20 ms; 0.6 and 04 signal fractions, respectively). Figure 2 (c) depicts the required t_{enc} for each k-space location. At the same readout bandwidth, zG_{RF}-RHE reaches every point in k-space faster than UTE due to gradient pre-ramping. The improved encoding efficiency across all k-space locations for any T_{RO} leads to better MTF characteristics and an overall shortened sampling duration. The t_{enc} gain depends on the system's dead-time. Single point measurements in zG_{RF}-RHE result in a constant t_{enc} (fixed at TE) in k-space center. Given the lower required gradient strength for longer T_{RO} the central k-space gap is smaller compared to faster readouts.

Figure 2 (b) and (d) show profile simulation results for UTE and zG_{RF}-RHE based on the MTF and t_{enc} for T_{RO} at 2 and 8 ms. The simulated profile and reconstruction results for UTE and zG_{RF}-RHE are illustrated in Figure 2 (b). Shorter readout leads to better reconstruction of the profile with less T_2 blurring artifacts. The higher encoding efficiency leads to an improvement in signal strength in zG_{RF}-RHE compared to UTE, particularly at longer T_{RO}. The finite difference illustration in Figure 2 (d) further emphasizes the better reconstruction of edge details at lower T_{RO}. zG_{RF}-RHE retrieves sharper edges at both investigated T_{RO}.

An analysis of the structural similarity index (sSim) between reconstructions and the original profile further underline the improvements of higher encoding efficiency. At T_{RO} = 2 ms, zG_{RF}-RHE simulation results achieved a sSim score of 0.95 compared to 0.94 for a standard UTE reconstruction. At T_{RO} = 8 ms, the profile reconstruction scores were 0.82 and 0.79 for zG_{RF}-RHE and UTE, respectively.

The phantom measurement analysis can be seen in Figure 3. The setup of phantom vials is depicted in Figure 3 (a). A comparison of UTE and zG_{RF}-RHE reconstruction results at the shortest investigated T_{RO} of 2 ms is shown in Figure 3 (c). Contour lines from normalized images illustrate sharper edges between tubes in zG_{RF}-RHE measurements at T_{RO} of 2 ms and a better delineation of small details (6 mm 45 mM in upper right corner). The mean line profile across the central slice of the 14 mm phantom tubes in short (2 ms) and long (8

ms) T_{RO} experiments is plotted in Figure 3 (b). Longer readouts lead to a reduction in overall signal strength due to more signal decay during sampling, however, the lower readout bandwidth also results in lower noise levels. At the same readout bandwidth, zG_{RF}-RHE achieves better signal due to the improved t_{enc} efficiency. Figure 3 (d) depicts the mean edge sharpness in 14 mm tubes across all phantom experiments. To exclude partial volume effects, edges were measured between the central voxel of the tube and 9.3 mm (3 voxel) to either side. The measurements underline the better edge definition at T_{RO} of 2 ms with decreasing sharpness towards longer readouts. Across all T_{RO}, zG_{RF}-RHE showed small edge enhancements for both sodium concentrations. SNR analysis results from a central region of the 28 mm tubes are displayed in Table 1. An average SNR increase of up to 4.8% was observed for zG_{RF}-RHE across all T_{RO} with significant gain at longer T_{RO}. Concomitant improvements in contrast-to-noise ratio (CNR) between 30 and 45 mM tubes were found.

Figure 4 (a) depicts cross sections through in vivo experiments. zG_{RF}-RHE showed better detail around the brain stem at short T_{RO}. CSF masks were segmented from proton-based FLASH images and registered to UTE and zG_{RF}-RHE sodium acquisitions using FSL. Figure 4 (b) shows three consecutive transverse cross sections of CSF segmentation masks through the ventricles. The overlay of contour masks of both acquisition techniques at T_{RO} = 2 ms reveals a better delineation of ventricle in zG_{RF}-RHE measurements.

Discussion

The fast biexponential decay properties of sodium need to be addressed with dedicated UTE sequences. Recent advancements in Sodium MRI focused on the improvement of sampling efficiency in k-space (13,16,17) which is an inherent drawback of fast center-out UTE acquisitions. While these measurement schemes enhance sampling homogeneity for an amelioration of point spread function characteristics and a potential total scan time reduction, the aspect of encoding time efficiency has not yet been explored. A quick signal detection onset is necessary for unbiased sodium concentration quantification in density-weighted acquisitions (30).

The enhanced time encoding scheme of zTE imaging cannot readily be applied in sodium MRI due to the generally low in vivo sodium concentration and the very limited attainable

flip angle under non-zero gradients and limited B1 power. The concept of hybrid encoding with separated acquisitions of central and peripheral k-space (akin to keyhole imaging) has been introduced in PETRA and generalized in RHE. PETRA and the proposed zG_{RF}-RHE encoding approach with gradient-free excitation and an immediate ramping can be seen as two special cases at opposite ends of the RHE spectrum.

This work utilizes the combination of radial and single point acquisition as originally proposed in PETRA (21). Froidevaux et al. (31) recently showed that this hybrid encoding strategy for dead-time gap filling generally achieves better image quality than other approaches, e.g. algebraic zTE (32), WASPI (33).

zG_{RF}-RHE preserves a homogeneous excitation profile facilitating high flip angle and improved encoding time for any receiver bandwidth (T_{RO}). Simulation and experimental measurements reflect the benefits of alleviated signal decay during sampling in SNR improvements and better encoding efficiency in reduced T_2^* blurring particularly at short T_{RO}. It should be noted that the observed SNR improvement results from a combination of factors, predominantly the improvement in MTF (cf. Figure 2), and secondly the avoidance of ramp sampling which is known to have lower SNR efficiency (16). This study applied a post-acquisition Hann filter during image reconstruction. Stronger SNR improvements are expected with a Sampling Density Weighted Apodization (SDWA) trajectory adjustment (34,35).

Gradient ramping prior to sampling onset leads to an acquisition gap in central k-space that needs to be filled retrospectively through single point measurements. Due to the commonly low resolution and relatively low readout bandwidth in sodium MRI the filling of central k-space components only requires a comparatively low number of single points. For the measurements presented in this work only up to 27 single points needed to be acquired. Based on the chosen TR of 160 ms this lead to an additional measurement time of 4.3 sec. In zG_{RF}-RHE, central k-space is measured at a fixed t_{enc} equal to the minimum achievable TE.

The single point measurements in zG_{RF}-RHE can be exploited to analyze eddy current related distortions and correct gradient imperfections as suggested by Jang et al. (23). While this correction has not been applied in this work, it can provide further image quality

improvements. Given the the moderate gradient strengths ramped during the dead-time, eddy current effects are, however, expected to be minor in this study.

This work examined the application of zG_{RF}-RHE in radial trajectories. The zG_{RF}-RHE timing concept is, however, not limited to radial sampling schemes but can in fact be used in combination with any center-out sampling pattern, e.g. density-adapted radial (16), TPI (13,14) or 3D cones (17). Since such sampling patterns commonly utilize higher initial gradients the resulting central k-space gap might, however, be slightly bigger. It should be noted that radial acquisitions provide the most efficient way to get to the edges of k-space at a given readout bandwidth and, hence, offer the greatest potential for T_2^* blurring reduction. Nevertheless, the low SNR regime and particular signal decay characteristics in Sodium MRI render the optimal T_{RO} and trajectory design a challenging choice. Due to the improved sampling homogeneity, twisted or density-adapted trajectories are expected to further improve image characteristics with regard to SNR.

Zero-gradient excitation (zG_{RF}) prevents any additional artifacts during excitation that result from gradient modulation during excitation. This is crucial in Sodium MRI, given its inherently low image quality. Recently, RHE has been applied in whole body MR/PET where volume-selective SLR pulses were used to mitigate excitation artifacts resulting from outside the field of view (33). In the current study we did not observe any unwanted excitation artifacts. Due to the unrealized efficiency, non-selective hard pulses are commonly employed in Sodium MRI acquisitions. Nevertheless it should be noted that the gradient-free excitation approach of zG_{RF}-RHE solely exploits the system's dead-time for encoding efficiency improvements. This excitation-independent efficiency gain brings great flexibility with it and facilitates the use of more elaborate excitation schemes beyond rectangular hard pulses.

A benefit of the akin hybrid sampling approach PETRA is the significant acoustic noise reduction due to the low gradient ramp time requirements for radial and single point acquisitions. It should be noted that this condition is not met in this RHE approach as a result of the gradient free excitation requirement – gradients need to be fully ramped up and down between repetitions of both radial and single point measurements. Nevertheless, the readout bandwidth in sodium MRI is commonly low for better SNR characteristics leading to moderate applied gradient strengths and associated acquisition noise.

The increased encoding efficiency results in slightly shorter total readout times for any readout bandwidth. In multi-echo data acquisitions the time gain allows for faster refocusing and consequently closer echo spacing which is beneficial for the estimation of signal decay parameter, in particular for the short T_2 decay component (27,37,38).
The zG_{RF}-RHE acquisition approach shows image quality improvements across investigated T_{RO}, while for shorter T_{RO} an improvement in edge delineation was observed, SNR improvements were found particularly for longer T_{RO}.
Other x-Nuclei of interest in biological tissue like Chlorine-37 and Oxygen-17 with spin >1/2 exhibit quadrupolar interactions characterized by short transverse relaxation times. It is anticipated that the concept of improved sequence timing concept with undistorted excitation conditions will provide benefits for such short-T2 x-Nuclei imaging applications, along with MSK applications for sodium imaging.

Conclusion

This work investigates zG_{RF}-RHE for a readout-independent improvement of encoding efficiency in sodium MRI under preserved non-selective high flip angle excitations. The presented encoding scheme combining pre-ramped radial acquisitions and single-point central k-space data achieves the highest encoding efficiency for any readout bandwidth and improves on image quality with regards to SNR and T_2^* blurring.
While this work investigated radial acquisition schemes, the optimised encoding time concept with hybrid encoding and gradient pre-ramping is applicable to any center-out trajectory design.

List of Figures

Fig 1: Radial zero-Gradient-Excitation Ramped Hybrid Encoding (zG_{RF}-RHE) Sequence Diagram (a) and 2D illustration of hybrid k-space encoding scheme (b). Gradient-free excitation is followed by an immediate gradient ramping, data sampling commences after dead-time. Central k-space is measured separately as single points with the same gradient pre-ramping condition. Echo Time, TE; Readout Duration, T_{RO}; dead-time t_d.

Fig 2: UTE and zG_{RF}-RHE sequence comparison for biexponential T2 decay ($T2_{short}$ = 1.5 ms, $T2_{long}$ = 20 ms).
Left: Modulation transfer function (MTF) (a) and encoding time (t_{enc}) (c) over k-space readout. Zoomed-in window illustrates reduced encoding efficiency during ramp up in standard UTE (red). Solid line indicates 2 ms T_{RO}, dashed line shows 8 ms T_{RO}.
Right: Profile simulation (b) and edge definition analysis (d). (b) Black line illustrates simulated profile, red line shows standard UTE, blue line indicates zG_{RF}-RHE results for T_{RO} = 2 ms (solid) and T_{RO} = 8 ms (dashed). (d) indicates finite differences of original profile and simulated reconstructions.

Fig 3: Phantom experiment.
Left: Illustration of phantom setup (a) and reconstructed images at T_{RO} = 2 ms (c) in UTE and zG_{RF}-RHE experiments. Upper rows show raw images at the native FOV, lower rows displays edge characteristics through zoomed in contour lines of normalized images.
Right: Mean line profiles (b) through 14 mm phantom tubes at shortest (2 ms, solid lines) and longest (8 ms, dashed lines) T_{RO} in UTE (red) and zG_{RF}-RHE (blue) experiments. Mean edge sharpness (d), i.e. finite difference between central voxel and neighbouring background voxel, in 14 mm phantom tubes at 45 mM (gray) and 30 mM (white) concentrations across all measured T_{RO}. Dashed line (left bars) indicates standard UTE measurement, solid line (right bars) shows zG_{RF}-RHE edges.

Fig 4: (a) Cross sections through matched slices in in vivo experiments at T_{RO} of 2 ms UTE and zG_{RF}-RHE. zG_{RF} -RHE shows sharper details around the brain stem (red arrow). (b) Three consecutive transverse slices of CSF masks with contour lines of normalized UTE and zG_{RF}-RHE at T_{RO} of 2ms. zG_{RF}-RHE provides better delineation between lateral ventricles (red arrow).

List of Tables

Table 1: Mean SNR and CNR in phantom experiments and significance measure.

Phantom – SNR												
	T_{RO} 2ms			T_{RO} 4ms			T_{RO} 6ms			T_{RO} 8ms		
	UTE	zG_{RF}-RHE	p-value	UTE	zG_{RF}-RHE	p-value	UTE	zG_{RF}-RHE	p-value	UTE	zG_{RF}-RHE	p-value
30mM	14.25 ±0.67	14.35 ±0.82	0.092	19.22 ±1.33	20.14 ±0.88	**0.013**	21.74 ±1.12	22.20 ±1.25	**0.001**	25.32 ±0.48	25.60 ±0.56	**0.005**
45mM	20.90 ±0.63	21.00 ±0.83	0.252	28.00 ±1.81	29.31 ±0.71	0.052	31.83 ±1.17	32.54 ±1.22	**0.018**	36.66 ±0.64	37.22 ±0.63	**0.006**
Phantom – CNR												
	T_{RO} 2ms			T_{RO} 4ms			T_{RO} 6ms			T_{RO} 8ms		
	UTE	zG_{RF}-RHE	p-value	UTE	zG_{RF}-RHE	p-value	UTE	zG_{RF}-RHE	p-value	UTE	zG_{RF}-RHE	p-value
30 to 45mM	7.14 ±0.26	7.22 ±0.36	0.226	9.10 ±0.55	9.75 ±0.19	**0.009**	10.3 ±0.52	10.75 ±0.54	**0.016**	11.22 ±0.22	11.63 ±0.32	**0.001**

Acknowledgements

We acknowledge the facilities, and the scientific and technical assistance of the Australian National Imaging Facility at the Melbourne Brain Centre Imaging Unit. The work was also supported by a research collaboration agreement with Siemens Healthcare.

Jon Cleary is funded by a University of Melbourne McKenzie fellowship. Brad Moffat is supported by the Australian National Imaging Facility (NIF).

References

1. Thulborn KR. Quantitative sodium {MR} imaging: {A} review of its evolving role in medicine. Neuroimage 2016.
2. Madelin G, Regatte RR. Biomedical applications of sodium {MRI} in vivo. J Magn Reson Imaging 2013;38(3):511-529.
3. Wetterling F, Gallagher L, Macrae IM, Junge S, Fagan AJ. Regional and temporal variations in tissue sodium concentration during the acute stroke phase. Magn Reson Med 2012;67(3):740-749.

4. Tsang A, Stobbe RW, Asdaghi N, Hussain MS, Bhagat YA, Beaulieu C, Emery D, Butcher KS. Relationship between sodium intensity and perfusion deficits in acute ischemic stroke. J Magn Reson Imaging 2011;33(1):41-47.
5. Schepkin VD. Sodium {MRI} of glioma in animal models at ultrahigh magnetic fields. NMR Biomed 2016;29(2):175-186.
6. Ouwerkerk R, Bleich KB, Gillen JS, Pomper MG, Bottomley PA. Tissue sodium concentration in human brain tumors as measured with 23{N}a {MR} imaging. Radiology 2003;227(2):529-537.
7. Nagel AM, Bock M, Hartmann C, Gerigk L, Neumann JO, Weber MA, Bendszus M, Radbruch A, Wick W, Schlemmer HP, Semmler W, Biller A. The potential of relaxation-weighted sodium magnetic resonance imaging as demonstrated on brain tumors. Invest Radiol 2011;46(9):539-547.
8. Maarouf A, Audoin B, Pariollaud F, Gherib S, Rico A, Soulier E, Confort-Gouny S, Guye M, Schad L, Pelletier J, Ranjeva JP, Zaaraoui W. Increased total sodium concentration in gray matter better explains cognition than atrophy in {MS}. Neurology 2017;88(3):289-295.
9. Inglese M, Madelin G, Oesingmann N, Babb JS, Wu W, Stoeckel B, Herbert J, Johnson G. Brain tissue sodium concentration in multiple sclerosis: a sodium imaging study at 3 {T}esla. Brain 2010;133(Pt 3):847-857.
10. Zbyn S, Mlynarik V, Juras V, Szomolanyi P, Trattnig S. Evaluation of cartilage repair and osteoarthritis with sodium {MRI}. NMR Biomed 2016;29(2):206-215.
11. Marik W, Nemec SF, Zbyn S, Zalaudek M, Ludvik B, Riegler G, Karner M, Trattnig S. Changes in {C}artilage and {T}endon {C}omposition of {P}atients With {T}ype {I} {D}iabetes {M}ellitus: {I}dentification by {Q}uantitative {S}odium {M}agnetic {R}esonance {I}maging at 7 {T}. Invest Radiol 2016;51(4):266-272.
12. Madelin G, Babb JS, Xia D, Chang G, Jerschow A, Regatte RR. Reproducibility and repeatability of quantitative sodium magnetic resonance imaging in vivo in articular cartilage at 3 {T} and 7 {T}. Magn Reson Med 2012;68(3):841-849.
13. Boada FE, Gillen JS, Shen GX, Chang SY, Thulborn KR. Fast three dimensional sodium imaging. Magn Reson Med 1997;37(5):706-715.

14. Lu A, Atkinson IC, Claiborne TC, Damen FC, Thulborn KR. Quantitative sodium imaging with a flexible twisted projection pulse sequence. Magn Reson Med 2010;63(6):1583-1593.
15. Nielles-Vallespin S, Weber MA, Bock M, Bongers A, Speier P, Combs SE, Wohrle J, Lehmann-Horn F, Essig M, Schad LR. 3{D} radial projection technique with ultrashort echo times for sodium {MRI}: clinical applications in human brain and skeletal muscle. Magn Reson Med 2007;57(1):74-81.
16. Nagel AM, Laun FB, Weber MA, Matthies C, Semmler W, Schad LR. Sodium {MRI} using a density-adapted 3D radial acquisition technique. Magn Reson Med 2009;62(6):1565-1573.
17. Riemer F, Solanky BS, Stehning C, Clemence M, Wheeler-Kingshott CA, Golay X. Sodium 23{N}a ultra-short echo time imaging in the human brain using a 3{D}-{C}ones trajectory. MAGMA 2014;27(1):35-46.
18. Weiger M, Pruessmann KP, Hennel F. M{RI} with zero echo time: hard versus sweep pulse excitation. Magn Reson Med 2011;66(2):379-389.
19. Heid OaD, M. Rapid {S}ingle {P}oint ({RASP}) {I}maging. 1995; Nice, France. p 684.
20. Balcom BJ, Macgregor RP, Beyea SD, Green DP, Armstrong RL, Bremner TW. Single-{P}oint {R}amped {I}maging with {T}1 {E}nhancement ({SPRITE}). J Magn Reson A 1996;123(1):131-134.
21. Grodzki DM, Jakob PM, Heismann B. Ultrashort echo time imaging using pointwise encoding time reduction with radial acquisition ({PETRA}). Magn Reson Med 2012;67(2):510-518.
22. Romanzetti S, Halse M, Kaffanke J, Zilles K, Balcom BJ, Shah NJ. A comparison of three {SPRITE} techniques for the quantitative 3{D} imaging of the 23{N}a spin density on a 4{T} whole-body machine. J Magn Reson 2006;179(1):64-72.
23. Jang H, Wiens CN, McMillan AB. Ramped hybrid encoding for improved ultrashort echo time imaging. Magn Reson Med 2016;76(3):814-825.
24. Saff EB, and Arno BJ Kuijlaars. Distributing many points on a sphere. The Mathematical Intelligencer 1997;19(1):7.
25. Zwart NR, Johnson KO, Pipe JG. Efficient sample density estimation by combining gridding and an optimized kernel. Magn Reson Med 2012;67(3):701-710.

26. Madelin G, Lee JS, Regatte RR, Jerschow A. Sodium {MRI}: methods and applications. Prog Nucl Magn Reson Spectrosc 2014;79:14-47.
27. Blunck Y, Josan S, Taqdees SW, Moffat BA, Ordidge RJ, Cleary JO, Johnston LA. 3D-multi-echo radial imaging of 23 {N}a (3{D}-{MERINA}) for time-efficient multi-parameter tissue compartment mapping. Magn Reson Med 2017.
28. Gudbjartsson H, Patz S. The {R}ician distribution of noisy {MRI} data. Magn Reson Med 1995;34(6):910-914.
29. Stobbe RW, Beaulieu C. Calculating potential error in sodium MRI with respect to the analysis of small objects. Magn Reson Med 2018;79(6):2968-2977.
30. Boada FE, Christensen JD, Huang-Hellinger FR, Reese TG, Thulborn KR. Quantitative in vivo tissue sodium concentration maps: the effects of biexponential relaxation. Magn Reson Med 1994;32(2):219-223.
31. Froidevaux R, Weiger M, Brunner DO, Dietrich BE, Wilm BJ, Pruessmann KP. Filling the dead-time gap in zero echo time {MRI}: {P}rinciples compared. Magn Reson Med 2018;79(4):2036-2045.
32. Kuethe DO, Caprihan A, Lowe IJ, Madio DP, Gach HM. Transforming {NMR} data despite missing points. J Magn Reson 1999;139(1):18-25.
33. Wu Y, Dai G, Ackerman JL, Hrovat MI, Glimcher MJ, Snyder BD, Nazarian A, Chesler DA. Water- and fat-suppressed proton projection {MRI} ({WASPI}) of rat femur bone. Magn Reson Med 2007;57(3):554-567.
34. Stobbe R, Beaulieu C. Advantage of sampling density weighted apodization over postacquisition filtering apodization for sodium MRI of the human brain. Magn Reson Med 2008;60(4):981-986.
35. Konstandin S, Nagel AM. Performance of sampling density-weighted and postfiltered density-adapted projection reconstruction in sodium magnetic resonance imaging. Magn Reson Med 2013;69(2):495-502.
36. Jang H, Liu F, Bradshaw T, McMillan AB. Rapid dual-echo ramped hybrid encoding MR-based attenuation correction (dRHE-MRAC) for PET/MR. Magn Reson Med 2018;79(6):2912-2922.
37. Ridley B, Nagel AM, Bydder M, Maarouf A, Stellmann JP, Gherib S, Verneuil J, Viout P, Guye M, Ranjeva JP, Zaaraoui W. Distribution of brain sodium long and short

relaxation times and concentrations: a multi-echo ultra-high field (23){N}a {MRI} study. Sci Rep 2018;8(1):4357.

38. Lommen JM, Flassbeck S, Behl NGR, Niesporek S, Bachert P, Ladd ME, Nagel AM. Probing the microscopic environment of 23{N}a ions in brain tissue by {MRI}: On the accuracy of different sampling schemes for the determination of rapid, biexponential {T}2* decay at low signal-to-noise ratio. Magn Reson Med 2018.

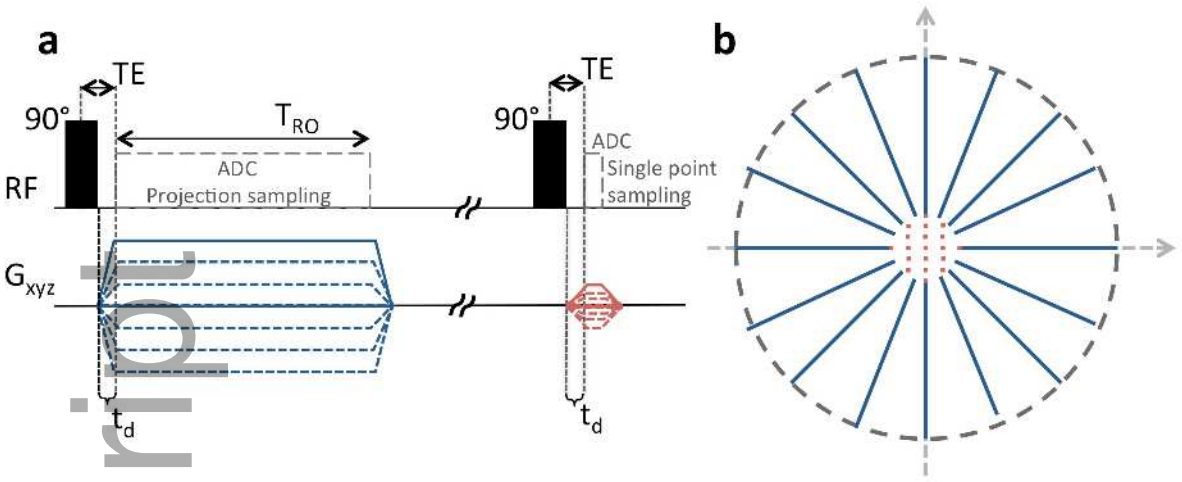

mrm_27484_f1.tiff

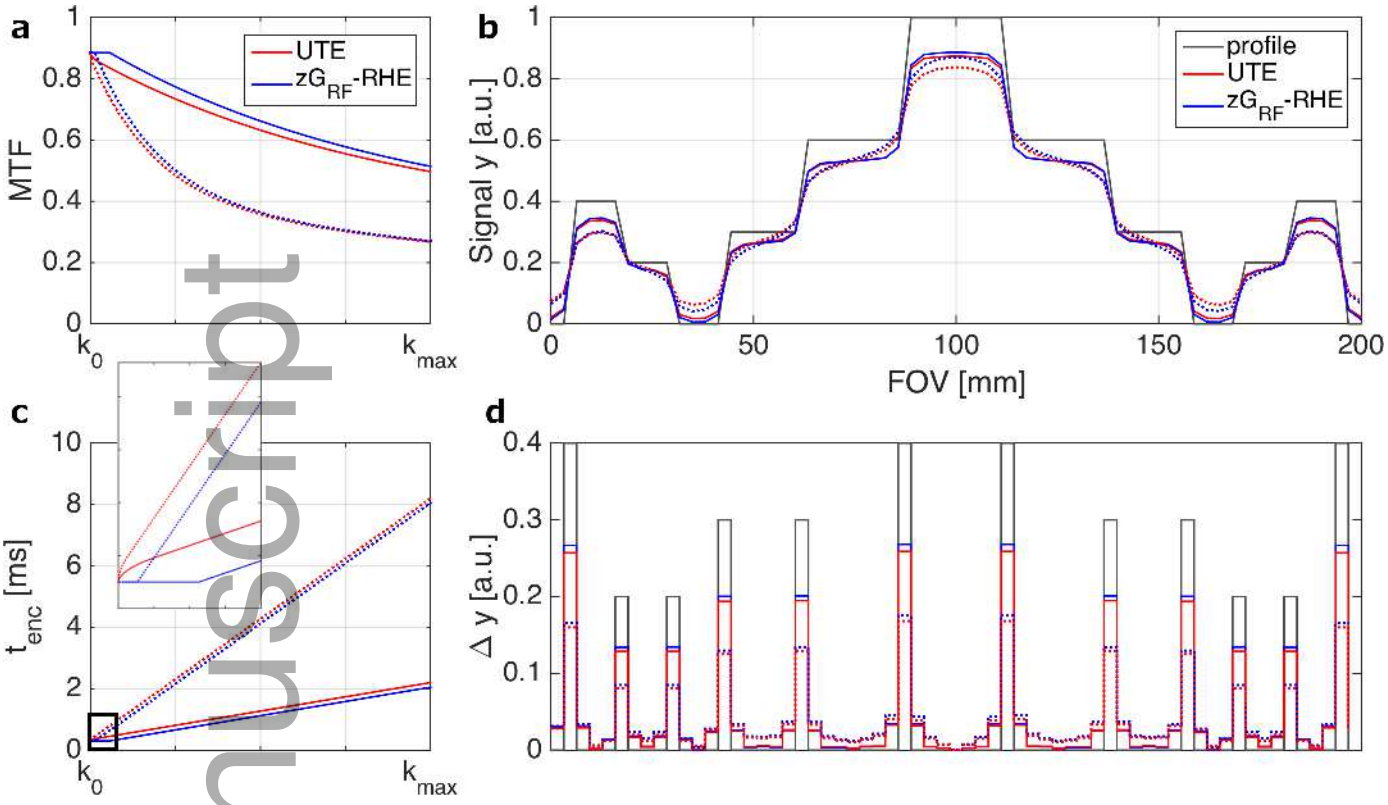

mrm_27484_f2.tiff

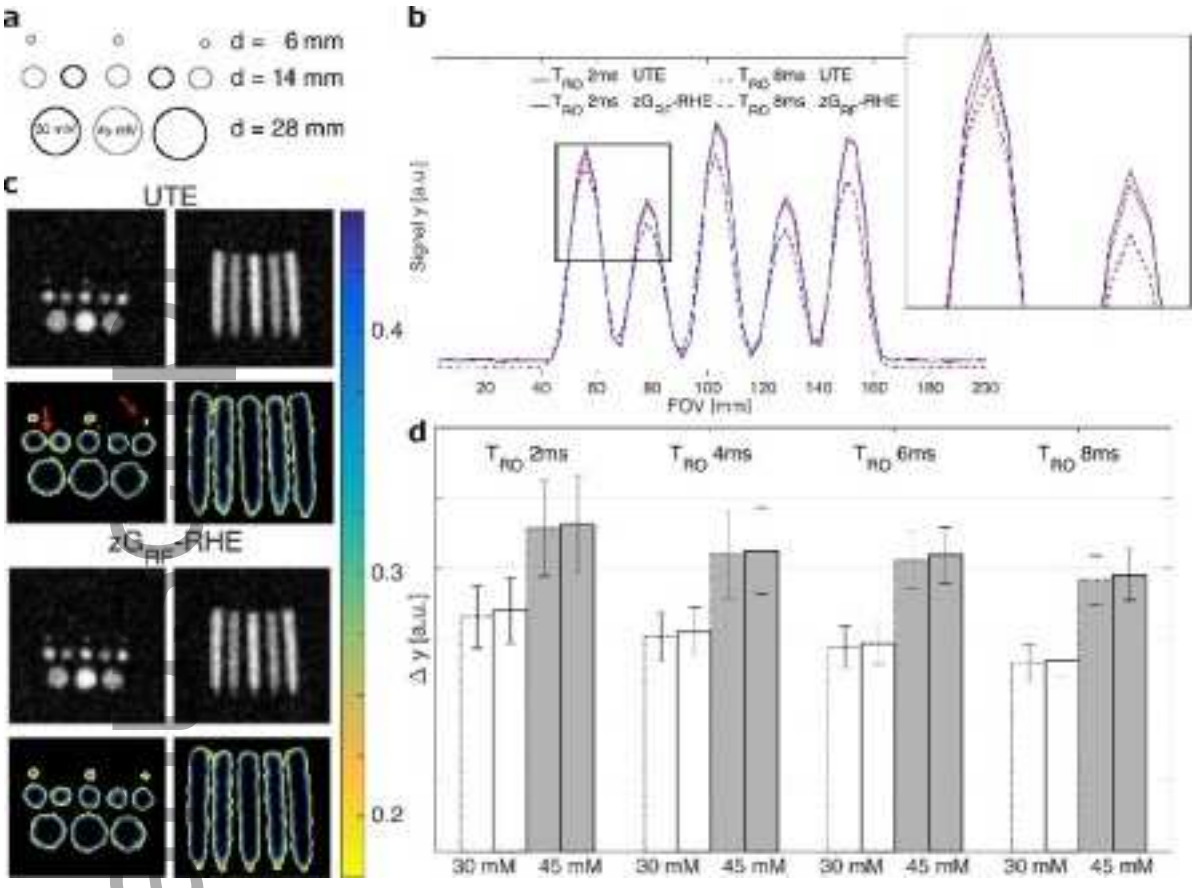

mrm_27484_f3.tiff

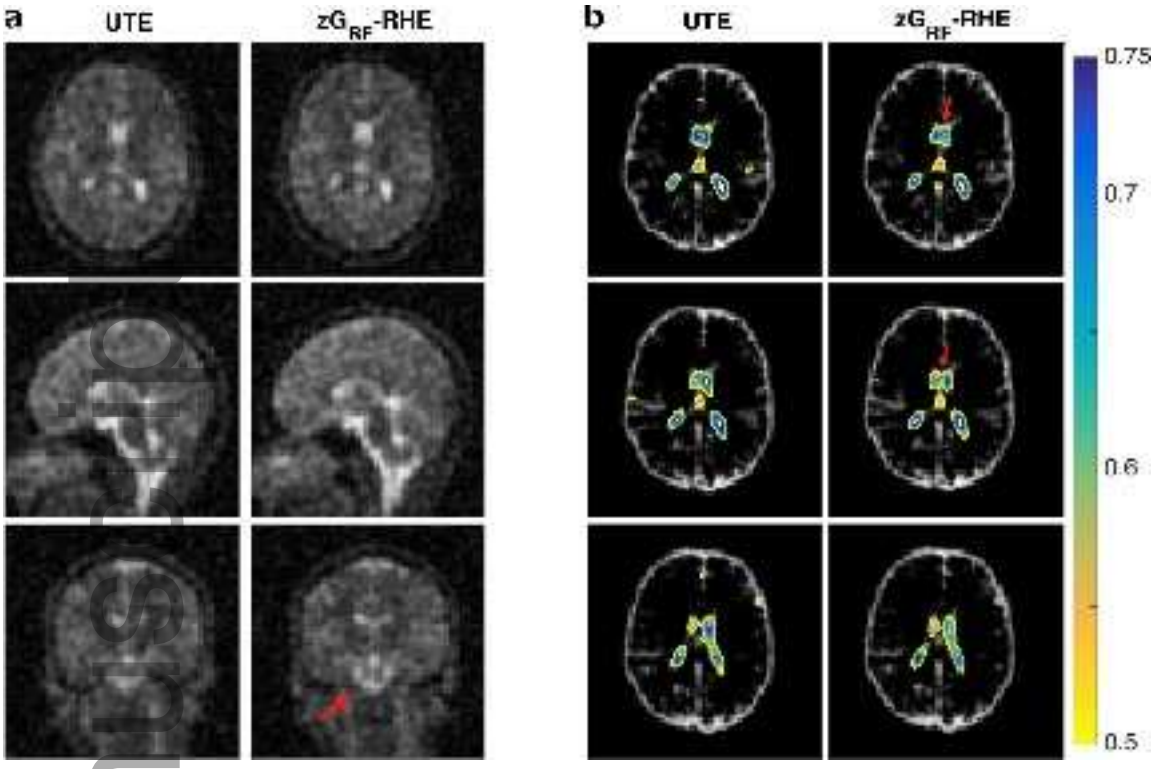

mrm_27484_f4.tiff